VERSITA

Acta Geophysica
vol. 56, no. 1, pp. 58-87
DOI: 10.2478/s11600-007-0049-8

Stable-boundary-layer regimes from the perspective of the low-level jet

Robert M. BANTA

NOAA Earth System Research Laboratory
Boulder, Colorado, USA
e-mail: robert.banta@noaa.gov

Abstract

This paper reviews results from two field studies of the nocturnal stable atmospheric boundary layer (SBL) over the Great Plains of the United States. Data from a scanning remote-sensing system, a High-Resolution Doppler Lidar (HRDL), provided measurements of mean and turbulent wind components at high spatial and temporal resolution through the lowest 500-1000 m of the atmosphere. This data set has allowed the characteristics of the low-level jet (LLJ) maximum (speed, height, direction) to be documented through entire nights. LLJs form after sunset and produce strong shear in the layer below the LLJ maximum or nose, which is a source of turbulence and mixing in the SBL. Simultaneous HRDL measurements of turbulence quantities related to turbulence kinetic energy (TKE) has allowed the turbulence in the subjet layer to be related to LLJ properties. Turbulence structure was found to be a function of the bulk stability of the subjet layer. For the strong-LLJ (> 15 m s^{-1}), weakly stable cases the strength of the turbulence is proportional to the strength of the LLJ. For these cases with nearly continuous turbulence in the subjet layer, low-level jet scaling, in which lengths are scaled by the LLJ height and velocity variables are scaled by the LLJ speed, was found to be appropriate. For the weak-wind (< 5 m s^{-1} in the lowest 200 m), very stable boundary layer (vSBL), the boundary layer was found to be very shallow (sometimes < 10 m deep), and turbulent fluxes between the earth's surface and the atmosphere were found to be essentially shut down. For more intermediate wind speeds and stabilities, the SBL shows varying degrees of intermittency due to various mechanisms, including shear-instability and other gravity waves, density currents, and other mesoscale disturbances.

Key words: stable boundary layer, low-level jet, Doppler lidar, atmospheric turbulence, turbulence kinetic energy.

1. INTRODUCTION

The stable boundary layer (SBL), like its unstable counterpart, has been studied for many decades, but progress in understanding and modeling it has been considerably slower. Suppressed mixing under stable conditions allows smaller-scale features to persist, thus complicating the flow. The suppressed vertical mixing also facilitates layering, so that near-surface measurements are often not representative of conditions aloft. Increased stratification produces smaller, weaker, less efficient turbulent eddies, resulting in longer time scales of adjustment to changes in larger-scale conditions. As a result of all these factors, many aspects of the SBL are nonstationary, so that more sophisticated analysis techniques are required to sort out the relevant processes (Vickers and Mahrt 2003, Mahrt and Vickers 2006). A common theme is that the SBL is very complex and may defy attempts at simplification. The search for overriding principles to provide perspective in interpreting this complexity has met with limited success, and in particular attempts to parameterize SBL processes for numerical weather prediction (NWP) continues to be a challenge (Mahrt 1998, 1999).

Turbulence in the SBL is created by shear but is diminished by the static stability. A cornerstone of many SBL studies is the concept of local height-independent, or "z-less" turbulence, according to which the vertical size of the eddies is limited by the stratification $\partial\theta/\partial z$ rather than the height above the surface, so that above some height the eddies no longer feel the effects of the surface (Obukhov 1971, Wyngaard and Coté 1972, Wyngaard 1973). The relevant length scale is the buoyant length scale $\ell_B = C\sigma_w/N$, which depends on the local stratification [where σ_w is the vertical velocity standard deviation, N, the Brunt–Vaisala frequency, and C an empirical constant (Brost and Wyngaard 1978)]. Following this reasoning, the concept of "local scaling" finds that all nondimensional ratios of turbulent quantities approach a constant value for sufficiently large values of the stability parameter z/Λ, where Λ is an Obukhov length L defined in terms of "local" fluxes, i.e., fluxes at the level of measurement (Nieuwstadt 1984).

Classifications of SBL structure and dynamics have been attempted, even though, acknowledging the complexity of SBL behavior, Mahrt (1999) cautions, "Any attempt to divide the stable boundary layer into a few classes or states…is an oversimplification".

Classification regimes have been based on such quantities as h/L (e.g., Holtslag and Nieuwstadt 1986); z/L (e.g., Mahrt *et al*. 1998, Mahrt 1999); and bulk Richardson number Ri_B (e.g., Mahrt and Vickers 2006, Grachev *et al*. 2005, Ohya 2001), where h is the height of the SBL; L is the surface-layer Obukhov length; $Ri_B = (g/\theta)(\Delta\theta/\Delta z)/(\Delta U/\Delta z)^2 = (g/\theta)(\Delta\theta\Delta z)/\Delta U^2$; θ is the potential temperature; U is the mean wind; g represents the effect of gravity; and Δ represents the vertical separation across the bulk layer. Van de Wiel *et al*. (2002a, b) have pointed out that Λ or flux-based schemes and those based on local gradients are based on variables that are internal to the SBL, whereas schemes based on bulk parameters across a layer (e.g., Ri_B) may be based on variables external to the SBL, if the layer extends from the surface to the top of the SBL. For many purposes, including NWP, it would be desirable to characterize SBL turbulence in terms of the largest-scale external variables possible. In

this spirit, Mahrt *et al.* (2001) defined a radiation *Ri* by replacing the lapse rate in the numerator with a function of the surface net radiation R_{net}, Vogelezang and Holtslag (1996) investigated the use of *U* at the top of the SBL in expressions for *h,* and Banta *et al*. 2003 defined a jet *Ri* by replacing the shear in the denominator by the quotient of the speed and height of the low-level jet. Even more basically, the mean wind speed at some level has been used to classify different types of SBL behavior, in much the same manner as a stability parameter. Banta *et al*. (2002) found categories of consistent SBL turbulence structure based on the mean LLJ speed, and Mahrt and Vickers (2006) found a similar relationship based on the mean wind speed at 2 m above ground level (AGL), noting a "reasonable prediction of the mean value of σ_w with information only on the wind speed". Many of the schemes tend to find three regimes, a weakly stable regime with strong winds, a transition (often intermittent) regime, and a strongly stable regime with weak winds and a very strong surface-based inversion.

Recently van de Wiel *et al.* (2002b, 2003) defined a two-dimensional space, where one dimension is the surface stress (as a proxy for the large-scale pressure gradient) and the other is the surface net radiation R_{net}. This scheme, in concept based completely on external forcing variables, effectively sorts the SBLs into three regimes, which he called the continuous-turbulence regime for the weakest stability, the intermittent regime, and the radiation regime for the strongest stability.

An issue is the role of the low-level jet (LLJ) and its evolution in the development of SBL turbulence. Bursts of turbulence observed near the surface in the middle of the night have been attributed in some studies to late-night accelerations of the LLJ, producing increased shear (e.g., Mahrt *et al.* 2001). Also a series of studies has been based on the premise that the height of the SBL is determined by an adjustment of the layer toward a critical value of Ri_B across the SBL (e.g., Hanna 1969, Mahrt 1981, Wetzel 1982, Vogelezang and Holtslag 1996). Measurements of LLJ evolution to test these suppositions have been hampered by relatively coarse resolution in time and in the vertical, and sometimes measurements are not even available below 100-200 m, where recent studies have shown a large percentage of LLJs may exist (Banta *et al*. 2002).

Two recent field programs have featured new remote sensing tools designed to document the structure and evolution of the LLJ and SBL at high resolution. One instrument capable of providing such measurements is the High-Resolution Doppler Lidar (HRDL) of the National Oceanic and Atmospheric Administration's Earth System Research Laboratory (NOAA/ESRL). HRDL is a scanning lidar system that was deployed to the 1999 Cooperative Atmosphere-Surface Exchange Study (CASES-99) campaign and to the 2003 Lamar (Colorado) Low-Level Jet Program (LLLJP-03) to study SBL processes. Analysis of the lidar data from these projects has allowed the evolution of LLJ structure to be related to the evolution and structure of turbulence and turbulent fluxes in the SBL. Findings from these projects have provided alternative views of LLJ-turbulence interaction processes. The purpose of the present contribution is to review these alternative views based on high-resolution observations of the SBL/LLJ and to extend the analysis where necessary to provide further insight into SBL structure and its dependence on stability. Following Mahrt and Vickers (2006)

and Banta *et al*. (2003), bulk Richardson numbers (Ri_B or the jet Richardson number Ri_J) will be used as the relevant stability parameter.

2. MOTIVATION AND BACKGROUND

2.1 Motivation

The need for better understanding of stable boundary layer processes arises from its frequent occurrence. The SBL occurs during roughly half of the diurnal cycle, over land surfaces at latitudes between the polar areas. In some key regions of the globe it is persistent, such as over cold water surfaces and in the polar regions, which have been identified as bellwether areas for global climate change. Surface exchange (source or sink activity) is a critical component of budgets of many meteorologically and climatologically important quantities, including momentum, heat, and trace species, such as water vapor, CO_2, O_3, NO_x, and many others. Emphasis on nighttime chemistry in recent air-quality field campaigns (e.g., Brown *et al.* 2007) has brought attention to the importance of the depth and intensity of turbulent mixing in determining reactant concentrations. Dispersion under stable conditions, overnight minimum temperatures, nighttime fog formation, and fire weather are but a few of the practical forecasting applications for SBL processes. Early-evening decoupling of the boundary layer from surface friction leads to acceleration and LLJ formation (Blackadar 1957), important for wind-energy (e.g., Kelley *et al.* 2004, Emeis *et al.* 2007) and atmospheric transport applications, such as air quality (e.g., McNider *et al.* 1988, Banta *et al.* 1998) and severe weather forecasting (Stensrud 1996, Song *et al.* 2005).

Even apart from the important applications that would benefit from a better knowledge of the SBL, meteorology has become increasingly reliant on numerical weather prediction (NWP) models. This is true on all scales, from relatively local, where emergency response (including recent emphasis on "homeland security") and air quality are important applications, to synoptic models used in daily weather forecasts, and up to global, multiyear climate models, which are producing forecasts of climate out to several decades, centuries, or more. It is therefore important for model predictions to be as accurate as possible for these important applications. Those with experience in verifying such predictions against observations, including the public which relies on media forecasts, which are in turn based on model predictions, and the operational forecasters who issue the forecasts, realize that these predictions are often in error – and quite often at crucial times.

The sometimes questionable reliability of NWP output is only partly a resolution issue, since even the finest-scale models have problems with some processes, such as surface exchange and stable mixing. The larger-scale models are also susceptible to inadequacies in the representation of radiation, land-surface interaction, cloud, and other processes. An especially insidious effect is a result of errors of the same sign. Even if tiny, such errors iterated over thousands or tens of thousands of time steps significantly contaminate the solution (Tripoli, G.J., personal communication). The rep-

resentation of SBL processes in current models produces these kinds of errors. For example, Zhong and Fast (2003) simulated a well measured case study using three different mesoscale models (MM5, RAMS, and meso-Eta), and all three exhibited a significant cold bias and other erroneous trends, when compared with near-surface measurements. Results such as these demonstrate that this is not a problem that forming ensembles of models is apt to cure, because models tend to use the same basic approach to many physical parameterizations (differing in detail), depending on the current state of the art (Mahrt 1998). Limitations of current modeled nocturnal SBL processes mean that the more nocturnal cycles in a model run, the greater the error introduced by these errant processes. It should be a high priority to repair these faulty model processes, or if not repairable (e.g., by inability to use required spatial resolution), to accurately assess the error being introduced by the inappropriate representations of the processes.

2.2 LLJ definition

In contrast to the jet stream, which is a maximum in the wind-speed profile at the top of the troposphere, a low-level jet is a wind maximum in the lower troposphere, usually in the lowest 1 to 1.5 km AGL. The definition of a LLJ varies from study to study, depending largely on the application being addressed, but also dictated by limitations of the data set (Bonner 1968, Hoecker 1963, Mitchell *et al.* 1995, Stensrud 1996, Whiteman *et al.* 1997, Banta *et al.* 2002, Zhong *et al.* 1996, Song *et al*. 2005). For example, in studies where advection of material (water vapor, pollutants) is important, the strongest and deepest wind-speed maximum, which may be 400-1000 m AGL, would be the appropriate feature to define as a LLJ. In these cases, to qualify as a LLJ, a wind maximum may be required to have a peak speed of at least 2 m s^{-1} greater than winds at levels both above and below the maximum or nose (e.g., Andreas *et al.* 2000). In some studies, a minimum wind speed requirement for qualification as a LLJ has also been imposed.

For our investigation of nocturnal LLJs, the most basic requirement is an acceleration of the wind profile over daytime mixed-layer speeds late on the previous afternoon. Since we are interested in the depth of the surface-based turbulence layer, it is very important to include those cases where the surface shear may be relatively weak but is still strong enough to generate such turbulence, and therefore, to include all cases where LLJ generated turbulence can affect surface fluxes. We experimented with definitions where decreases of 0.5, 1.0, and 1.5 m s^{-1} above and below the jet nose were required for a LLJ, with little difference in results (Banta *et al.* 2002). No minimum speed is imposed.

2.3 SBL depth

The BL depth h has been a controversial issue. One can recognize three aspects of this problem: the definition of BL, determination or measurement of h, and modeling h. For purposes of this study the most fundamental definition of boundary layer will be that layer adjacent to the Earth's surface that interacts with the surface via turbulent fluxes over a period of about an hour, corresponding to one of the definitions sug-

gested by Beyrich *et al.* (1997), Seibert *et al.* (2000), and Balsley *et al.* (2006). The SBL is a special case of BLs, so properties that characterize BLs are also shared by SBLs. The one hour time condition allows the definition to apply even to intermittent BLs, such as the very stable BL (Smedman 1988, Mahrt and Vickers 2006, Banta *et al*. 2007), which will be described in greater detail in Section 3.2. The top of the BL is a level of minimum to negligible turbulence and fluxes, which isolates the rest of the atmosphere from the BL, as indicated in idealized profiles of BL structure derived from conceptual models developed empirically (e.g., Fig. 1 and right panel of Fig. 2).

Determination of *h* from measured data depends on what kinds of data are available. Ideally *h* would be determined from vertical profiles of turbulent quantities. In this study such high-quality turbulence profile measurements are available, so they will be used to determine *h*. The minimum in the profiles of turbulence variables was routinely observed at a level above the surface, so this level is taken to represent the BL top, consistent with the idealized profiles (e.g., Figs. 1-2).

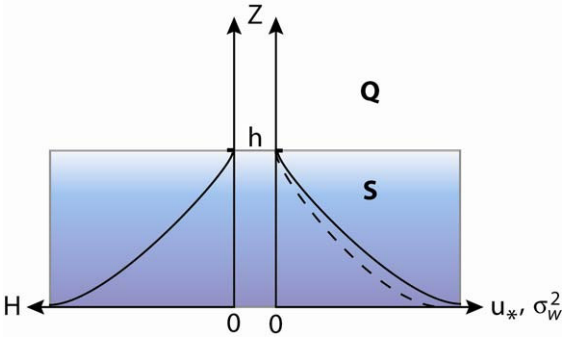

Fig. 1. Schematic profiles of heat flux H, vertical velocity variance σ_w^2, and friction velocity u_* showing "traditional BL" structure. Shaded portion marked *S* represents the stable boundary layer, and the region above marked *Q* represents a quiescent layer of weaker turbulence aloft. See color version of this figure in electronic edition.

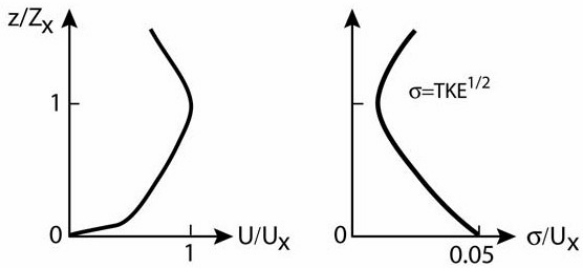

Fig. 2. Schematic profiles of: normalized mean wind speed $U(z)/U_x$ showing LLJ structure (left), and normalized standard deviation $\sigma(z)/U_x$ showing minimum at $z/Z_x = 1$ (right).

In general, however, h has been diagnosed from vertical profiles of various mean quantities, such as $\theta(z)$, wind speed $U(z)$, moisture, aerosol, and many others, largely because profiles of turbulent quantities have been difficult to obtain and are thus often unavailable. Indicators of h from mean profiles, such as inversion depth, or depth of the layer of high moisture or aerosol concentrations, are a result of surface-based turbulent mixing processes, and thus may or may not reflect the basic turbulence-based definition of the BL. Profiles of some quantities indicate effects related to processes other than turbulent mixing. For example, radiative flux divergence is important in the formation of θ profiles, which can produce inversions that extend above h. Larger-scale pressure gradients, which may affect U profiles within the BL, may include a diurnal height-dependent evolution especially near mountainous terrain, seacoasts, or other land-use boundaries. Moreover, in practice all profiles are susceptible to horizontal advection. Therefore, profiles of mean quantities must be interpreted with caution, as pointed out by Beyrich (1997), Seibert *et al.* (2000), and others.

Because turbulence profiles are not routinely available, it is worthwhile to consider and evaluate the use of more convenient measurables in determining h. During the CASES-99 and Lamar projects we observed that the minimum in turbulent variance profiles calculated from HRDL scan data corresponded very closely to the height of the LLJ nose Z_x (Fig. 3). On that basis we associated the LLJ height Z_x with the top of the SBL h. This relationship is in accord with Mahrt *et al.* (1979), who called the height of the jet maximum the "top of the momentum boundary layer", based on routinely observing a maximum in the gradient Ri at that level, as calculated from rawinsonde data taken during several field projects. The jet nose thus sits at the top of a layer of strong shear that is intimately interrelated to the strong BL turbulence. Because of this tight relationship between the surface-based layers of high turbulence and strong shear, the mean shear profile could therefore also be used as a diagnostic for h in the SBL, by noting at what level the shear first becomes small (e.g., Balsley *et al.* 2006).

Wind-speed profiles often exhibit multiple maxima, so we have specified the first local maximum in the wind profile above the surface layer as Z_x, which is intended to represent the top of the surface-based shear layer. The wind profile has often been observed to be nearly linear between the top of the surface layer and Z_x. However, we also noted some profiles regularly exhibited a sharp decrease or discontinuity in the shear at some level below Z_x (see Fig. 4). Although these profiles tended to occur during times of transition, the corresponding turbulence profile showed well developed SBL vertical structure with a top of the SBL at the height of the discontinuity in the shear. This suggests a further refinement or generalization of the definition of the SBL height as the height of the first peak negative value above the surface layer of the curvature or second derivative $\partial^2 U/\partial z^2$.

Finally, modeling the SBL depth, which is important for NWP applications, is another way that h can be expressed in terms of more conveniently measured variables. Several diagnostic formulations have been proposed. The widely used expression $h = c(Lu_*/f)^{1/2}$ (Zilitinkevich 1972), subsequently generalized by Zilitinkevich and Mironov (1996), uses variables in the surface layer, which can be measured by tower-

mounted instrumentation. Recently Steeneveld *et al.* (2007) used dimensional analysis to generate other formulations for h, some of which were found to perform well.

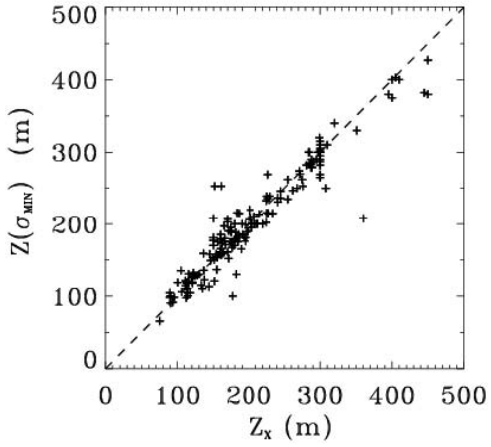

Fig. 3. Scatter diagram of height $z(\sigma_{min})$ of the minimum in the $\sigma_u(z)$ profile *versus* height of LLJ maximum Z_x (from Banta *et al*. 2006).

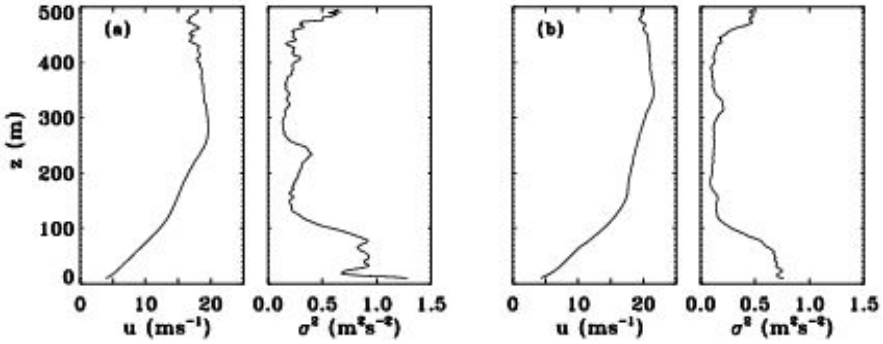

Fig. 4. Profiles showing a change in shear with height in the mean wind profiles (left panels) and the resulting cap in the strong turbulence at that level (right panels, streamwise variance), for (a) 06:50 UTC 5 September 2003, (b) 06:40 UTC 15 September 2003.

A different approach to modeling h has been to use a bulk Ri across the SBL, and assume that the SBL adjusts its depth to maintain a critical value of that Ri_B

$$Ri_{BC} = (g/\theta)\Delta\theta h / U_h^2 , \tag{1}$$

where Ri_{BC} is the critical bulk Ri, h is the top of the BL, and U_h is the wind speed at h (Hanna 1969, Mahrt 1981, Wetzel 1982, see Vogelezang and Holtslag 1996). Assigning a value to Ri_{BC} allows (1) to be solved for h in terms of the differences in θ and U

across the bulk layer. Thus an important question addressed in many of these studies is, what is the appropriate constant value of Ri_{BC}, to which the SBL heights adjust? This issue will be further discussed later.

The height of the LLJ maximum Z_x was found to be correlated to the speed of the jet maximum U_x (Banta *et al.* 2002). We also found Z_x to correspond to the height h of the turbulent SBL. Our Z_x-U_x correlation thus agrees with Vogelezang and Holtslag (1996), who found, using data from the 200-m Cabauw tower in the Netherlands, that the wind speed at the top of the SBL was well correlated with the SBL depth h, with a correlation coefficient of 0.85. They did not, however, find h to be well correlated with the surface layer friction velocity u_*, with a correlation coefficient of only 0.49 for the same dataset, and 0.69 for a somewhat larger dataset. Attempts to relate surface-layer u_* to U at the top of the SBL yielded poor correlations (Vogelezang and Holtslag 1996, Banta *et al.* 2006), the former reference finding a correlation coefficient of 0.44. Anecdotally, Mahrt (personal communication) has long observed that measured turbulence variables in the stable surface layer (especially u_*) are very erratic and often poorly related to gradients because of the variety of processes occurring there (see Mahrt and Vickers 2006, p. 36; Banta *et al.* 2007, and 2006, p. 2709), but above the surface layer the SBL may be much better behaved. This would explain why better correlations are obtained with wind speed or other variables above the surface layer than with u_*, which is measured within the atmospheric surface layer. It may explain some of the scatter in some of the diagnostic formulations for h. It also suggests that the wind speed at the top of the SBL may prove to be a better velocity scale for the determination of SBL height than u_*.

2.3 Instrumentation, datasets, and analysis techniques

The results described in this review were obtained from two field experiments in the Great Plains of the United States. The following description has been excerpted from Banta *et al.* (2006).

The CASES-99 field campaign consisted of a significant deployment of surface, airborne, and remote-sensing instrumentation to study the nocturnal stable boundary layer, as described by Poulos *et al.* (2002). One of the instruments deployed was the high-resolution Doppler lidar (HRDL) described by Grund *et al.* (2001) and Wulfmeyer *et al.* (2000). HRDL emits and receives backscatter from IR-light pulses, which are used to probe the aerosol-backscatter and Doppler-velocity structure of the atmosphere. The range of HRDL during CASES-99 was generally 1-2 km, the spatial resolution of the velocity measurements was 30 m in range, and the velocity precision was ~10 cm s^{-1}. HRDL data have been used in CASES-99 studies of LLJ and turbulence structure (Banta *et al.* 2002, 2003, 2006, 2007), atmospheric waves (Blumen *et al.* 2001, Newsom and Banta 2003, Fritts *et al.* 2003, Sun *et al*. 2004), density currents (Sun *et al*. 2002), late-afternoon near-neutral boundary-layer structure (Drobinski *et al.* 2004, 2007), and as a dataset for demonstrating four-dimensional variational data assimilation (4DVAR) techniques for Doppler lidar (Newsom and Banta 2004a, b).

HRDL was also a key instrument in the Lamar Low-Level Jet Project of 2003 (LLLJP-03), which was organized to investigate nocturnal SBL winds at a site being developed for wind energy. The formation of LLJs during nighttime is very important to wind-energy operations, providing enhanced wind speeds to drive the turbines. However, significant nocturnal bursts of turbulence can also adversely impact turbine hardware (Kelley *et al.* 2004). To address these issues, a late-summer field project was organized in early September 2003 at a High Plains location south of the town of Lamar in southeastern Colorado (Kelley *et al.* 2004, Pichugina *et al.* 2004, Banta *et al.* 2004). LLLJP-03 instrumentation included a 120-m tower instrumented at 4 levels and a 3-component Doppler sodar operated over two summers, and HRDL, which was deployed from September 1 through 16. The tower instruments included three-axis sonic anemometers mounted at heights of 54, 67, 85, and 116 m to provide three-component wind and temperature data at a sampling rate of 20 Hz, and mean temperature and wind data were taken at 2 Hz at 2 m. Nighttime HRDL data were collected from local sunset (~01:00 UTC) until 10:00-12:00 UTC, which was just before sunrise.

Bulk Richardson numbers were calculated from the tower data as described in Banta *et al.* (2003). The vertical differences in the bulk *Ri* calculation were determined from 1-min means of sonic anemometer data between the 25- and 55-m levels of the CASES-99 tower and between the 54- and 85-m levels of the Lamar tower. Gradient *Ri* values were also computed between adjacent levels of the CASES tower above 15 m and between adjacent levels of the Lamar tower. These *Ri* values generally tend to vary little with height and are about equal to the bulk value, as a result of the roughly linear profiles of U and θ between the top of the surface layer and Z_x, as previously noted.

The lidar scanning procedure generally employed during CASES-99 and LLLJP-03 was to perform repeated elevation ("vertical-slice") scans aligned with the mean wind direction for periods of 10-20 min or more. The mean wind direction was determined in real time by first performing 360° conical azimuth scans and then using the velocity-azimuth-display (VAD) technique (Browning and Wexler 1968, Banta *et al.* 2002).

A full 360° conical scan typically took ~2 min to complete, and the vertical-slice scans, about 30 s or less, depending on the resolution desired and thus the scanning speed selected. An example of vertical-slice scan data from the Lamar project is shown in Fig. 5. In general the data exhibited a LLJ maximum (e.g., in Fig. 5, it is at ~350 m). Analysis of the elevation-scan sequences consisted of assigning measurement data to vertically stacked bins at a constant height interval Δz, then averaging over all data in each of the horizontally oriented bins (as on Fig. 5). For profiles of the mean wind, bins of $\Delta z = 5$ or 10 m have provided estimates that agree well with wind speed profiles from towers, radar wind profilers, and balloon-borne anemometry. This agreement was routinely independent of the temporal averaging employed. However, for estimating the streamwise variance σ_u^2 in the stable, strongly sheared nocturnal conditions during these projects, Banta *et al*. (2006) and Pichugina *et al*. (2008) found that smaller vertical binning of $\Delta z = 1$ m was required for agreement with tower-measured streamwise variances or TKE.

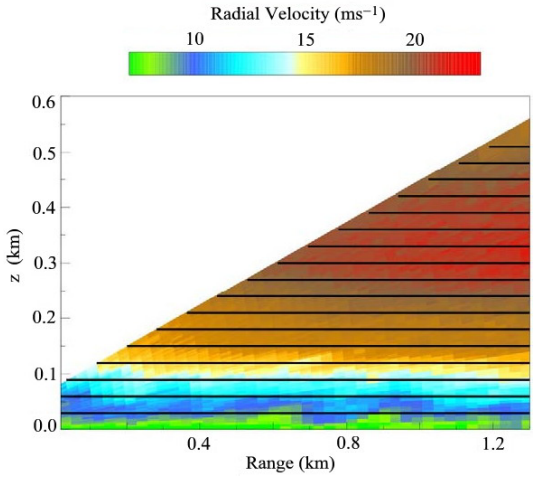

Fig. 5. Vertical-slice scan for 03:33 UTC on 9 September 2003 during the Lamar project, illustrating the vertical binning procedure. Vertical axis is height (km), horizontal axis is horizontal distance from the HRDL position at (0,0), which is to the left of the plot, and the color bar indicates wind speed (m s^{-1}). Means and variances were calculated over data within each horizontal band and assigned the height of the midpoint of each band to form vertical profiles. Width of each band Δz depicted here is 30 m for illustration, but actual intervals used for analysis were 10, 5, and 1 m (from Banta *et al*. 2006). See color version of this figure in electronic edition.

For the tower data from the CASES and Lamar datasets, TKE was calculated over 1-min intervals, and 10-min means were then calculated by averaging 10 consecutive 1-min values, analogous to the procedure devised and recommended by Vickers and Mahrt (2003). For the vertically binned HRDL data, temporal averaging was also applied using 5- and 10-min intervals. Regression analysis of the 5-min data yielded correlation coefficients r^2 of better than 0.75 for the entire dataset, and exceeding 0.8 for several individual nights of the study (Pichugina *et al*. 2008).

Comparisons of HRDL *versus* tower turbulence measurements pitted the variance component σ_u^2 against the total TKE on the tower. Banta *et al.* 2006 found using data from published SBL experiments that σ_u^2 is proportional to TKE, and that in fact, the proportionality constant is approximately 1 for stable conditions. Although further investigation is warranted, these calculations indicate that σ_u^2 and TKE should be nearly interchangeable in the SBL. σ_u^2 measured here is at least the major component of the TKE.

Another factor is directional shear in the LLJ flow. In the stronger-wind Great Plains cases studied here, veering with height occurred, but was routinely less than 30° across the subjet layer, which is not enough to affect the conclusions drawn here. When larger veering occurred, it was often associated with nonstationary or baroclinic conditions. Slow veering in time was also noted, qualitatively consistent with the inertial oscillation (Lundquist 2003). This veering was routinely from a southeasterly direction (150-160°) just after sunset to a southwesterly direction (220-230°) eight hours

or so later. This veering was slow enough that it did not seem to affect the equilibrium between turbulence and mean-SBL structure, as argued by Caughey *et al*. (1979) and Nieuwstadt (1984) for other forms of large-scale nonstationarity.

Advantages of this dataset are that Doppler lidar scan data are available at ~30-s intervals. The individual 10-min profiles are averages over data from many scans obtained during the interval, and they therefore represent more than 30-s "snapshot" profiles from individual scans. Having such averaged profiles available for entire nights provides the ability to observe the evolution of the LLJ structure and SBL turbulence.

3. REGIMES OF SBL-TURBULENCE INTERACTION

Plots of TKE as a function of different forms of bulk *Ri* revealed three regimes as shown in Fig. 6, a strong-wind weakly stable boundary layer (wSBL, indicated W) at small *Ri*, a weak-wind, very stable boundary layer (vSBL, indicated S) at large *Ri*, and a transitional regime (shaded vertical region) in between (Banta *et al*. 2003, 2006, 2007). The two forms of bulk *Ri* in these studies are a bulk *Ri* defined over a layer somewhere between the surface layer and Z_x, and the jet *Ri*, in which the shear in the denominator is estimated as U_x/Z_x. The $U(z)$ and $\theta(z)$ profiles have been found often to be roughly linear between the top of the surface layer and Z_x for these datasets, so that Ri_B and Ri_J tend to be nearly equivalent (except that sometimes Z_x is difficult to determine when the wind-speed profile is nearly constant above the surface-shear layer). Other implications of the near-linear profiles is that Ri_B is generally independent of the levels over which it is evaluated, so long as those levels are between the surface layer and Z_x, and Ri_B was about equal to the gradient *Ri*'s within that same layer.

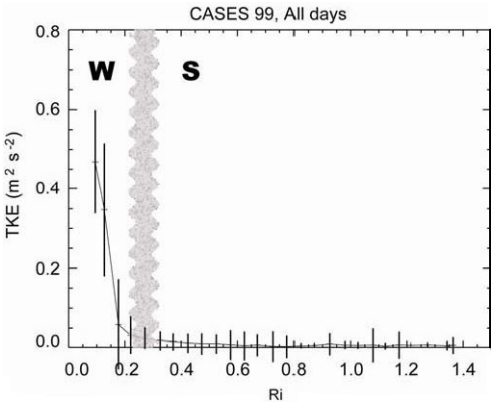

Fig. 6. Plot of TKE *versus* bulk *Ri* from Banta *et al.* (2006). TKE data were from near the top of the CASES-99 60-m tower, and *Ri* was calculated between the 5 and 55 m levels on the tower. TKE data were averaged for *Ri* intervals of 0.05 using the same data and technique as in Banta *et al*. (2003). Curved solid line connects the median values of TKE for each *Ri* bin, and vertical error bars indicate ±1 standard deviation for data in each bin. W indicates the weakly stable regime considered in this study, and S denotes the strongly stable regime. The vertical shaded region shows the approximate extent of the transitional regime.

3.1 Strong LLJ: the weakly stable BL

An example of the evolution of the wind-speed profile on a night with a strong LLJ is shown in Fig. 7. For these datasets, strong-wind nights are those nights when the LLJ speed exceeds 15 m s^{-1} at some time during the night (Banta *et al.* 2006). Using the high temporal resolution of the HRDL scan data, the evolution of the wind profile can also be documented on a time-height plot (Fig. 8). On the night in Fig. 8, the speed and height of the jet continued to grow through the night, but many nights more resembled Fig. 7, where the speed accelerated for the first 2-3 hr during the evening transition period and then became relatively steady or slowly varying for the rest of the night (Fig. 9).

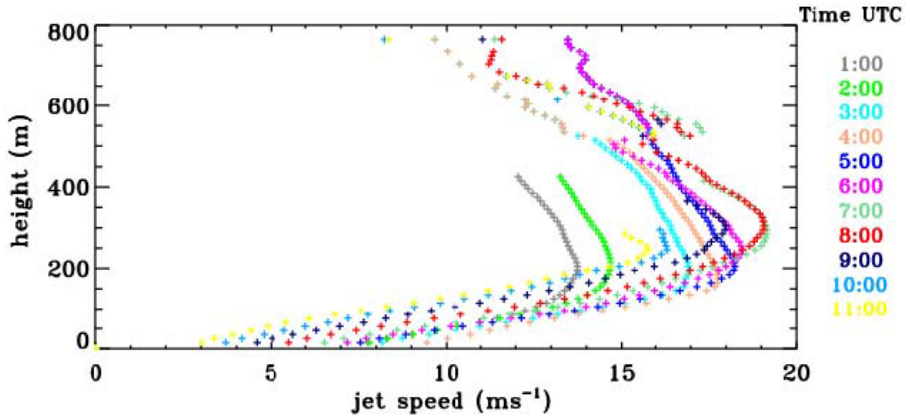

Fig. 7. Serial hourly-averaged profiles of the developing LLJ on 5 September 2003, calculated from HRDL scan data. Profiles that extend to lower altitudes were from time periods when lower-elevation scanning was being performed. See color version of this figure in electronic edition.

The acceleration of the LLJ after sunset produces strong shear in the layer below the jet. It is of interest that, as the LLJ in Fig. 7 grows in speed and height, the subjet shear remains about the same, i.e., the speed profiles are roughly linear and nearly parallel to each other. This shear in the subjet layer is strong enough to generate turbulence, strongest near the surface and with minimum values at the top of the SBL, which Mahrt (1999) refers to as 'traditional' BL structure (Fig. 2, right). In our studies, this minimum in turbulence at the top of the layer closely coincides with the nose of the LLJ, where the vertical shear goes to zero, as described in Section 2.3, indicating that the height of the LLJ maximum speed should be regarded as the top of the SBL (at least from the viewpoint of the vertical extent of surface-based turbulence and mixing). Figure 2 illustrates schematically this relationship between the mean and turbulent profiles, where the heights are scaled by the LLJ height Z_x and velocities are scaled by the maximum jet speed U_x. An example of the relationship between the LLJ height and turbulence using HRDL data over an entire night, for the same night as in Fig. 7, is given in Fig. 10, which shows a time-height plot of σ_u^2 with the height of the

LLJ (+ signs) superimposed. Similar plots for 15 September 2003 (the night shown in Fig. 8; Pichugina *et al.* 2004) and 6 September 2003 (Emeis *et al.* 2007) show this same behavior. The LLJ nose appears to cap the stronger turbulence in the subjet layer.

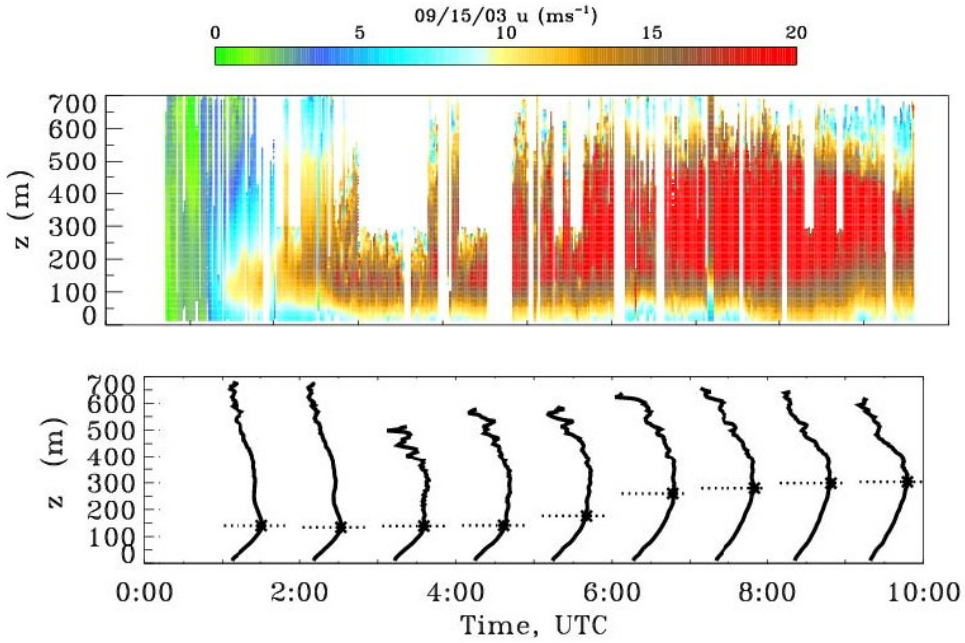

Fig. 8. *Top* Time-height cross section of wind speed for 15 September 2003, calculated from HRDL scan data. Color bar at top indicates wind speed in m s^{-1}. *Bottom* Hourly-averaged wind profiles corresponding to times in the top panel; asterisk symbols indicate peak LLJ speed and height, and horizontal dotted line in each profile extends from 5 to 25 m s^{-1}. Vertical axis is height above ground in both panels. Shorter profiles represent data from shallower scans.

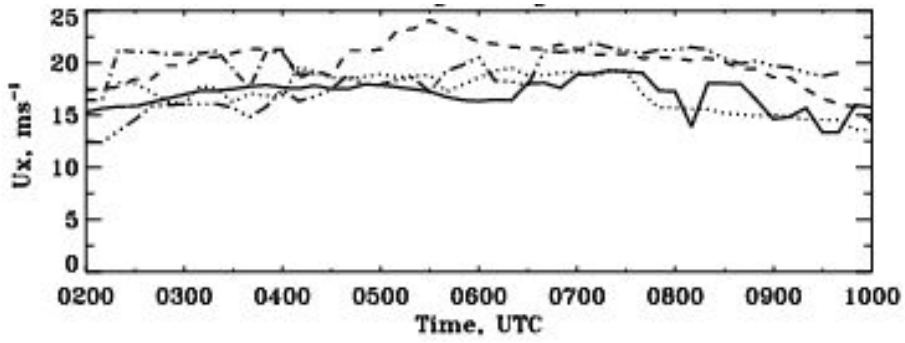

Fig. 9. Time series U_x for the four strong-wind study nights of the Lamar 2003 study.

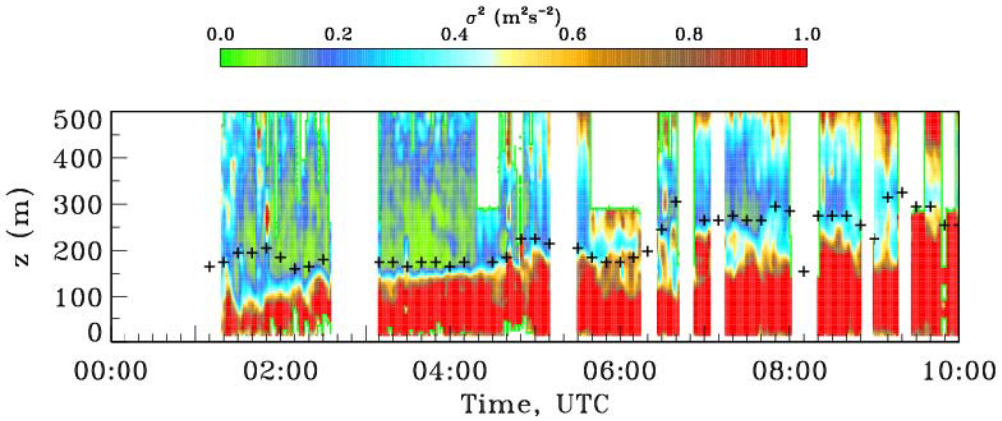

Fig. 10. Time-height cross section of streamwise velocity variance σ_u^2 for 5 September 2003 with the height of the jet Z_x superimposed (black + signs). Color bar at top indicates σ_u^2 values in m^2s^{-2}. LLJ height estimates (+) during blank periods are from conical scans using VAD processing, for which σ_u^2 estimates are not available but Z_x can be determined.

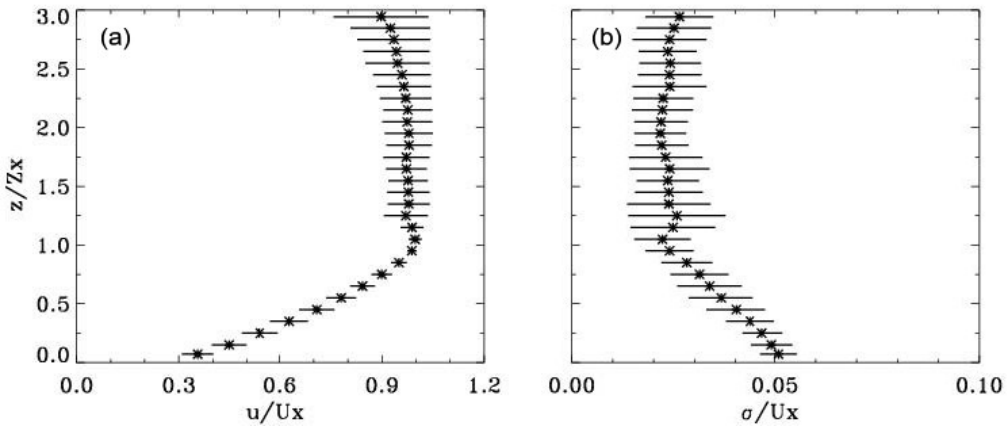

Fig. 11. Composite mean profiles of (a) normalized wind speed $U(z)/U_x$, and (b) normalized streamwise standard deviation σ_u $(z)/U_x$ for profiles where the maximum σ_u was at the surface (SX: Surface maXimum). Error bars represent plus/minus one standard deviation of the plotted variable calculated from the composite sample (from Banta *et al*. 2006).

HRDL-scan velocity data were binned and averaged over 10-min intervals. The 10-min profiles were then used to form composite vertical profiles, as described in Section 2.4, after scaling by U_x and Z_x. An example of the composite profiles for the data sample with traditional BL structure is shown in Fig. 11. The fit of the σ_u data (right panel), as indicted by the one-standard-deviation error bars, appears quite good for atmospheric turbulence data. The fit of the $U(z)$ profiles is also very good, but less impressive, because it is constrained to pass through (0,0) at the bottom and (1,1)

at Z_x. Profiles of σ_u normalized by U_x were also compared against those where $\sigma_u(z)$ was scaled by the surface-layer friction velocity u_*, the traditional scaling for turbulent momentum variables. The fit of the U_x-scaled profiles was better than the fit of those scaled by u_*, especially near the height of the LLJ maximum and also near the surface – where u_* is measured (Banta *et al.* 2006).

In addition to marking the top of the surface-based turbulent layer, therefore, Z_x is also an effective scaling depth for mean and turbulence variables. Thus, associating Z_x with the top of the SBL seems appropriate from both perspectives.

The turbulence profiles in Fig. 2 and Fig. 11 show a maximum of σ_u/U_x at the surface decreasing with height, but many profiles were also found with a layer of some depth having constant σ_u/U_x below the LLJ, and many more with a maximum above the surface, usually at heights of about 40-80 m AGL (Banta *et al.* 2006). The latter profile shape means that near the ground, the magnitudes of TKE or other turbulence quantities increase with height (Smedman *et al*. 1993, 1997, Mahrt and Vickers 2002, Banta *et al.* 2002, Balsley *et al.* 2006), which Mahrt (1999) has called an 'upside-down' boundary layer structure, because the primary source of turbulence appears to be aloft instead of at the surface (Fig. 12). Although LLJ structure was evident in the mean-wind profiles for all cases, a difference in stability was noted between the sample of profiles exhibiting traditional turbulence structure and those with upside-down structure. The traditional sample had a mean bulk Ri of 0.15, and the upside-down sample was somewhat more stable, with a mean Ri_B of 0.19, a difference found to be statistically significant. The mean for the sample with a constant σ_u/U_x layer was between the other two at 0.17 (Banta *et al.* 2006). This dependence of profile shape on stability has also been noted in wind-tunnel studies of the stably stratified BL (Ohya *et al.* 1997, Ohya 2001).

A somewhat surprising aspect of the composite σ_u/U_x profiles is the maximum value near the surface, which is shown in Fig. 11 to be 0.05. This value was the same for all stratifications of the dataset tried, including composites of each of the six individual nights of the sample and that for the composite of the entire dataset (Banta *et al*. 2006). A survey of previous studies for which σ_u and U_x could be determined revealed a mean value of this ratio over all these studies of 0.04, which was regarded as good agreement. Another way of stating the relationship expressed by this ratio is that the maximum of σ_u below the jet is 5% of U_x, indicating that the peak turbulence magnitudes below the LLJ are controlled by the speed of the LLJ, or equivalently, by the difference in U across the subjet layer.

Time series of several variables for the same night as in Figs. 7 and 10 are shown in Fig. 13, which illustrate the behavior seen on many strong-wind nights, as follows. The LLJ speed (top panel) levels off after ~02:00 UTC (about 2 hours after sunset) – after the evening transition period, showing some variation after 06:30 UTC. The height of the jet is more variable. The subjet shear and lapse rate (middle panel) also level off after the transition period, exhibiting random-appearing variations about a steady mean value for most of the night. The bulk Ri (bottom panel) also remains relatively steady after the transition period at a value of just greater than 0.10, with small

variations. It is difficult to make a case that the variations of Z_x are clearly an adjustment to bring Ri_B back to a critical value, but if such a value existed, all strong-wind nights examined indicate that it would have to be ~0.11-0.12. Although Ri_B was near this value for much of the evening, on some nights after ~08:30 UTC (1½ or 2½ hours after local midnight), Ri_B became even smaller as a result of a late-night drop in the lapse rate.

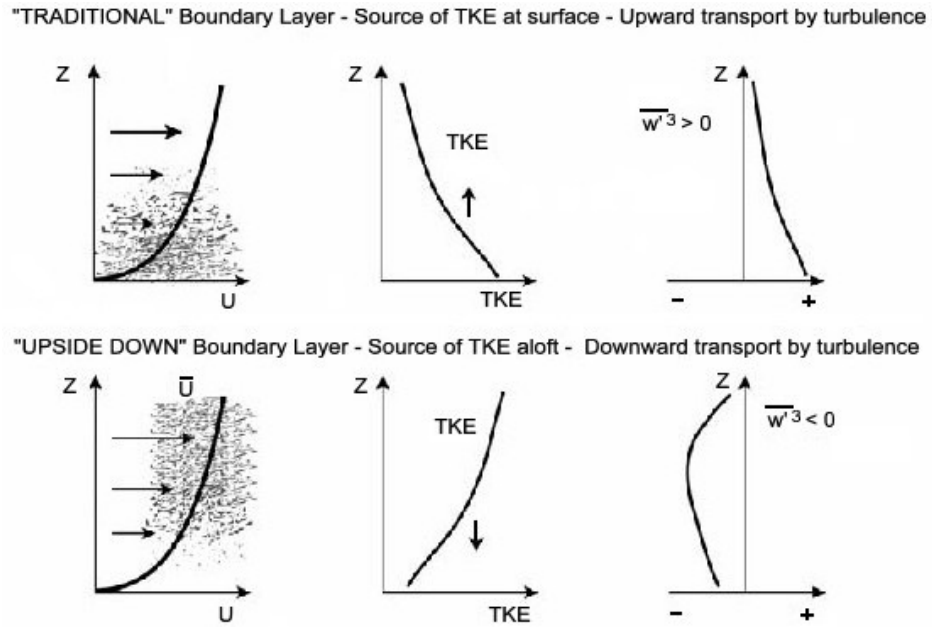

Fig. 12. Schematic structure of traditional boundary-layer (top) *versus* upside-down boundary-layer (bottom) according to criteria of Mahrt and Vickers (2002), i.e., that TKE (or other velocity variances) increase with height and σ_w^3 is negative through the upside-down layer. Left panels show mean horizontal wind-speed profiles with turbulence regions shaded; center panels show TKE or velocity-variance profiles; and right panels show vertical turbulent transport of TKE ("triple-correlation") term in TKE budget, of which σ_w^3 is a component (from Banta *et al.* 2006).

In summary, the use of a new remote sensing tool, the High-Resolution Doppler Lidar, has enabled turbulence measurements to be made in layers above those normally accessible to tower-mounted instrumentation, and this has produced an alternative view of the strong-wind SBL. Some implications of these findings are:

- The LLJ is an integral part of the wSBL.
- LLJ properties, including speed and height, must be measured in field projects studying the SBL.
- NWP models must properly represent the LLJ speed, height to calculate accurate turbulent fluxes "for the right reasons".

- Turbulence near the surface below the jet is primarily controlled by large-scale meteorological processes, which determine the LLJ speed.
- The turbulent SBL below the LLJ has properties of a similarity boundary layer in which the mean-wind speed and height of the top of the SBL, which generally corresponded to the LLJ maximum, are the appropriate velocity and height scales for both mean and turbulent quantities.

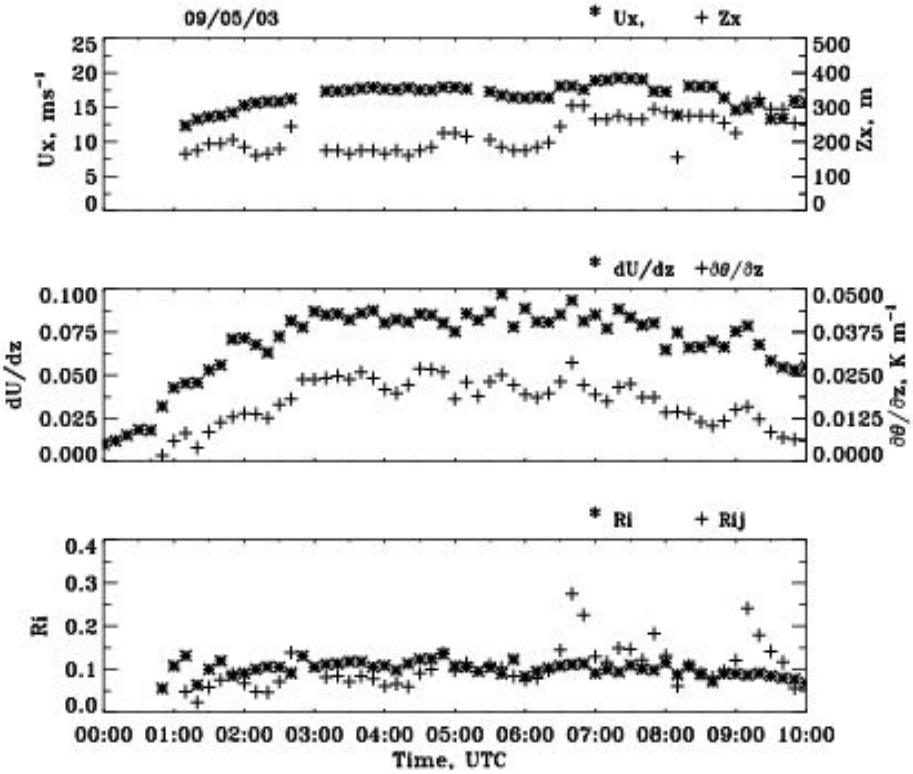

Fig. 13. *Top panel* Time series of U_x(*) and Z_x(+) calculated from 10-min average HRDL profiles; (middle panel) mean shear (*) and lapse rate (+) calculated from sonic anemometer data for the 54-85-m layer on the 115-m tower at Lamar. *Bottom panel* Ri_B (*) calculated from 54 to 85 m differences in tower data, and Ri_J (+) calculated from both HRDL and tower data, 5 September 2003.

3.2 Weak winds: the very stable BL

When the winds in the lowest 200 m are light (probably less than ~5 m s^{-1} for our arid Great Plains data set), strong surface cooling is confined to a shallow layer of the atmosphere, producing very strong stability. For example, Ri_B values in excess of 20 were observed on a relatively calm night during CASES-99 (cf. Fig. 5 of Banta *et al.* 2003). Although these conditions are often associated with calm or light-and-variable

winds at the surface, Banta *et al*. (2007) found that vertical profile shapes could persist in the winds above the surface for periods of 1 hr or more. Since these profiles often exhibit jet-like structure even though the peak speeds could be less than 2 m s^{-1}, it is reasonable to generalize that these strongly stable BLs tend to be associated with weak LLJs.

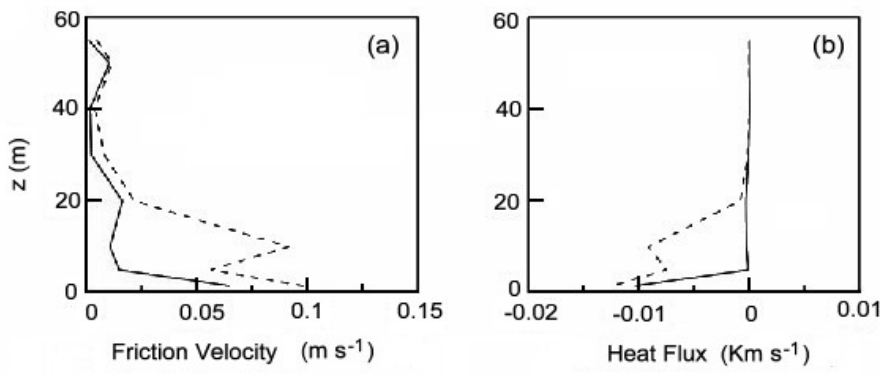

Fig. 14. Profiles of 60-min averaged u_* and *H,* from sonic anemometers on the 60-m CASES-99 tower, averaged according to the Vickers and Mahrt (2006) procedure, showing traditional BL structure beneath quiescent layer for hours beginning 04 and 07 UTC (22 and 01 CST) (solid, dashed) on 18 October 1999: (a) friction velocity u_*, and (b) kinematic heat flux *H* (from Banta *et al.* 2007).

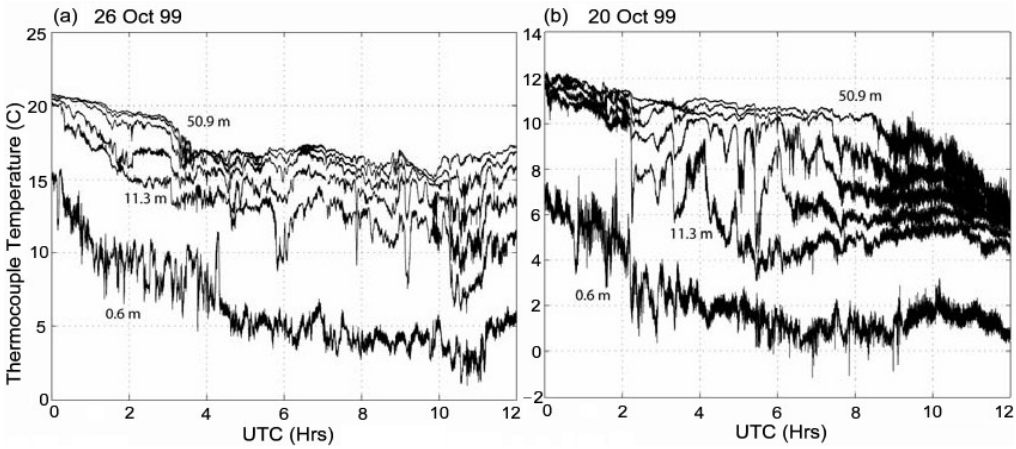

Fig. 15. Thermocouple time series (*T* in °C, obtained at 5 Hz) at 6 levels of the CASES-99 tower for (a) 26 October 1999, and (b) 20 October 1999. On 20 October the significant cooling at the upper tower levels starting at ~08:00 UTC (and very evident after 09:30 UTC) was a result of an air-mass change and increased wind speeds. Measurement heights were 0.63 m, 11.3 m, 20.3 m, 29.3 m, 40.1 m, and 50.9 m (from Banta *et al*. 2007)

The SBL in these instances is often less than 25 m deep, and may be less than 10 m deep (Smedman 1988, Mahrt and Vickers 2006, Banta *et al.* 2007), as shown in the CASES-99 tower data in Fig. 14. The turbulence in this shallow SBL is weak and intermittent, and is best studied using specialized analysis procedures that account for the nonstationarity of the processes (Vickers and Mahrt 2003, Mahrt and Vickers 2006). Also shown in Fig. 14 is the fact that in the layer just above the shallow SBL, the turbulent fluxes become so small as to be negligible. The effect of this second "quiescent" stratum above the shallow BL was demonstrated using high-frequency temperature T data from the CASES-99 60-m tower (Fig. 15). The T traces at the lower tower levels, which were within the shallow SBL, show cooling and large-amplitude fluctuations. The upper tower levels were in the quiescent layer aloft, and those traces show dramatically reduced fine-scale structure and the temperature leveling off for several hours in the middle of each night – an indication that cold air near the surface was not being mixed up to the higher tower levels. Thus, although the prevailing view has been that some mixing occurs between the surface and the atmosphere due to one mechanism or another in the vSBL, these tower data do not support this view. In these cases, a quiescent layer completely isolates the surface from the atmosphere above the shallow SBL (Fig. 16). This suggests that for NWP applications the appropriate lower boundary condition for fluxes, representing the interaction between the surface and the atmosphere, may be to allow these fluxes to approach or become equal to zero (Banta *et al.* 2007).

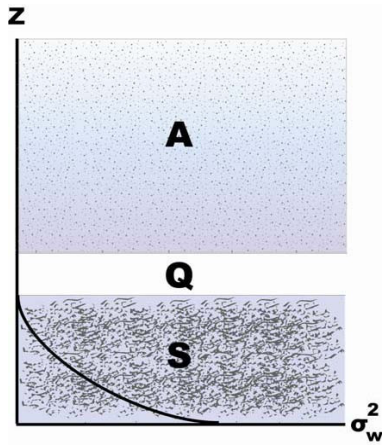

Fig. 16. Schematic representation of shallow BL, S, quiescent layer Q, and atmosphere above quiescent layer A, showing the vertical relationship between the two lowest atmospheric layers (S and Q) and the atmosphere above A. The region A (which may include the remnants of the previous afternoon's mixed layer and the free atmosphere) is not addressed in this study, but most likely consists of many layers itself, at least some having intermittent turbulence. The important finding was that in the vSBL atmospheric properties at the surface or in S are not transported by any means up into region A (from Banta *et al*. 2007).

Several nights with marginally stronger winds were available in the CASES-99 data set. In Banta *et al.* (2007) the same kind of vSBL structure just noted was found for most hours of these nights, but with interruptions by intermittent mixing events. For example, a night with a 7 m s^{-1} jet exhibited propagating gravity-wave and density-current activity (18 October 1999: Sun *et al.* 2002, 2004), and another night with a 9 m s^{-1} jet was interrupted by a traveling shear-instability (Kelvin–Helmholtz-type) wave packet (5 October 1999: Blumen *et al*. 2001, Poulos *et al.* 2002, Newsom and Banta 2003). This dataset thus suggests a progression with decreasing stability, in which a two-stratum (shallow BL plus quiescent layer) vSBL structure forms on nights when winds are less than 5 m s^{-1} below 200 m, but then, as wind speeds increase from nights having 6 m s^{-1} LLJs to those with 10 m s^{-1} jets, this structure is interrupted by increasing occurrence, intensity, and perhaps duration of intermittent disturbances, as well as changes in the character of those disturbances.

3.3 Intermediate / transition SBL

Continuing the progression to wind speeds greater than 10 m s^{-1}, a night with a 12 m s^{-1} jet began with vSBL structure, but then featured a strong downward burst of turbulence and upside-down structure for several hours starting at ~02:00 LST (08:00 UTC) on 14 October 1999 (Balsley *et al.* 2006, Banta *et al*. 2007). This case illustrates the behavior seen on nights when LLJ speeds were between about 10 and 15 m s^{-1}. Early in the evenings the boundary layers exhibit the very stable structure, but after several hours – between about 23:00 and 02:00 LST – a downward burst of strong turbulence and mixing typically occurs, lasting a few hours. For example, Fig. 17 shows this kind of "bursting" activity between 05:00 and 08:00 UTC (23:00 and 02:00 LST) on 21 October 1999, a CASES night with an 13 m s^{-1}. LLJ previously described by Banta *et al.* (2002) and Ha and Mahrt (2001). This type of activity during CASES-99 has been documented during the 14 October case already mentioned (Balsley *et al.* 2006,

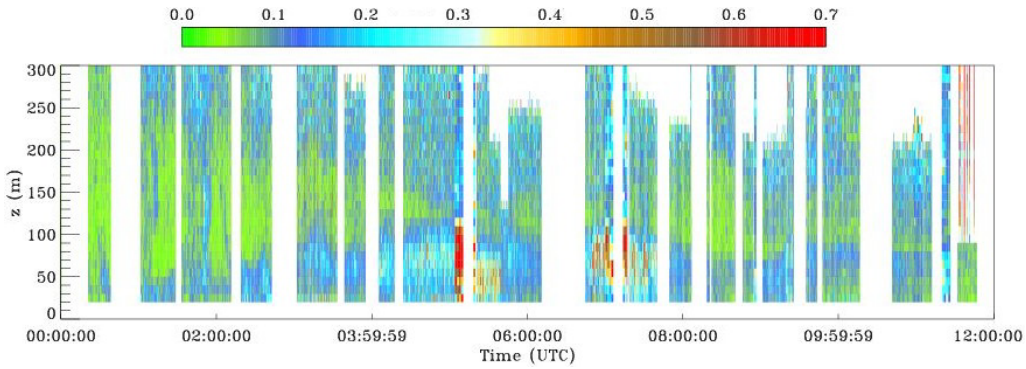

Fig. 17. Time-height cross section of σ_u^2 for the CASES-99 night of 24 October 1999 (UTC), showing bursts of turbulence below the LLJ between 06:00 and 08:00 UTC. Colorbar shows σ_u^2 scale in m^2 s^{-2} (Banta *et al*. 2002).

Banta *et al.* 2007), and also found on the nights beginning at 00:00 UTC on 23 October (Mahrt and Vickers 2002) and 27 October 1999. Previous studies (most recently van de Wiel *et al*. 2002a) have noted that this transitional regime is the one characterized by a cycle of stabilization and acceleration-destabilization that produces intermittent turbulence. Further study of the nights with this intermittent behavior is needed.

4. DISCUSSION: POTENTIAL IMPLICATIONS

The findings reviewed in the previous section have emphasized a low-level-jet view of the SBL. The basic behavior of the turbulence in the subjet layer is a function of a bulk or jet *Ri*. Vigorous mixing and traditional BL structure were noted at the weak stability, small *Ri* extreme and a shallow, weakly turbulent BL with no surface-atmosphere turbulent interaction prevailed at the strongly stable, large *Ri* extreme. Between the two extremes we noted a regime of various degrees of intermittency near the critical value of Ri_B or Ri_J, in agreement with other classification schemes in the literature. The transition behavior appears to lie between Ri_B or Ri_J values of about 0.2 and 0.3 (Fig. 6; Banta *et al*. 2003).

Within the strong-jet, wSBL regime, modest increases in stability produced an elevation of the maximum in the turbulence profile from the surface (traditional structure) to a level ~40-80 m above the surface ("upside down" structure). This behavior could be associated with the tendency of the cases with modestly increased stability to be associated with lower jet speeds, and therefore smaller TKE (and associated turbulent fluxes) near the surface, than the weaker-stability, stronger-LLJ cases. The θ profile near the ground, on the other hand, is controlled by the surface energy budget, which consists of processes resulting both from forcing external to the SBL and from processes within or at the lower boundary of the SBL.

The externally forced terms in the surface energy budget – net radiation and exchange with the ground or canopy surface – are independent of wind speed and thus would be the same in both cases (assuming clear skies and similar soil moisture, vegetation, and other conditions at the lower boundary). The surface energy budget could be expressed as (neglecting evaporation and dew or frost formation, i.e., latent-heat effects):

$$\partial\theta_0/\partial t + \left(\partial <w\theta> /\partial z\right)_0 = R_{net} + Fg \quad , \tag{2}$$

where θ_0 is the potential temperature at the roughness height, $<w\theta>$ the kinematic heat flux, R_{net} the net radiation, and Fg the heat flux into the ground or canopy layer. The terms on the right side are the externally forced terms, representing a cooling potential. The left side of the equation can be viewed as a response within the SBL to the external forcing. Here for a given value of the cooling potential, a smaller contribution by the term representing a flux to the atmosphere would mean greater surface cooling in time, and greater static stability. Thus, nights with somewhat weaker jets, larger *Ri*, and weaker near-surface turbulent fluxes would have colder surface temperatures, larger static stability in the lower part of the subjet layer, and greater buoyant suppres-

sion of TKE and other turbulence quantities. Because $\partial\theta/\partial z$ is strongest near the surface, the suppression of turbulence would also be strongest there leading to smaller values of TKE near the ground, increasing with height as $\partial\theta/\partial z$ becomes smaller. The shift to a peak in turbulence above the surface ("upside-down" structure) at slightly larger Ri_B in the wSBL is thus attributed to a reduced contribution by turbulent heat fluxes on the left side of (2), requiring stronger cooling for a given value of the right side. This enhanced cooling produces greater stability and greater suppression of the turbulent fluxes at the lowest levels of the subjet layer.

The observations have shown that subjet turbulence magnitudes are proportional to U_x. The explanation for this could be that stronger jets systematically produce stronger shear, but this is not supported by the observations: stronger jets tend to be higher so that the shear is often about the same magnitude between periods with strong jets (> 15 m s^{-1}) and those with more moderate jet speeds (9-14 m s^{-1}) (e.g., Fig. 7, also Banta *et al*. 2003). If the shear varies little, the alternative explanation for the relationship between turbulence and U_x is that the large-eddy size (or mixing length) scales with the layer depth, i.e., Z_x. The argument would be that the larger eddies in the deeper, stronger-jet SBLs would be mixing air at greater vertical separation having greater differences in U, even though $\partial U/\partial z$ was similar. This implication that the turbulence scales with the jet height and thus "feels" the depth between the surface and the level of the LLJ maximum would seem to contradict z-less and local similarity arguments.

5. CONCLUSIONS

Mean wind and turbulence data obtained in the lowest kilometer of the atmosphere from two field projects over the U.S. Great Plains have allowed the mean and turbulent structure of the nocturnal LLJ to be documented at vertical resolutions of 10 m or less with individual 'instantaneous' profiles available at time intervals of as little as 30 s, which were then averaged over 5, 10, or 15-min intervals. Composite analyses of the profiles of the mean wind speed and the streamwise variance σ_u^2, which was argued to be equivalent to TKE for stable conditions, produced well-defined profiles with reasonably small scatter when heights were normalized by the height of the LLJ and velocity variables, by the speed of the jet maximum. This "LLJ scaling" has been effective for the wSBL and for the transitional, intermittent SBL during periods when downward bursts of turbulence were occurring.

The analyses also showed that the near-surface maximum of σ_u is proportional to the wind speed at the nose of the LLJ, with a proportionality factor of 0.05. Shear was not found to be systematically different between strong-jet cases with weak stability, and somewhat weaker-jet cases with modestly stronger stability, as the stronger-jet cases tended to be associated with higher jets. It was noted that this dependence of turbulence magnitude near the surface with LLJ speed may imply that the large-eddy dimensions (or mixing lengths) scale with the depth of the layer between the surface

and the jet maximum, and that this appears to conflict with the local scaling concept, which holds that the large eddy sizes are controlled only by the local stratification.

The search for simplifying points of view for interpreting SBL behavior has achieved some apparent success at the strong-wind, weak stability extreme and at the weak-wind, very stable extreme. The results in the previous two paragraphs describe findings for the former regime, which was found to be characterized by traditional, similarity BL structure for the cases with the weakest stabilities. This type of boundary layer seems to be well represented by a basic stably-stratified wall flow, and laboratory measurements have shown reasonable success in reproducing the behavior we found here. The latter, strongly stable extreme was characterized by a very shallow boundary layer, with the exchange between the surface and the atmosphere above the shallow boundary layer shut down by an essentially "dead layer" of extremely weak turbulence just above the shallow BL. The regimes between the two extremes are characterized by varying degrees and types of intermittency. Moving in stability (Ri_B or Ri_J) space (or alternatively with decreasing wind speed) from the weak-stability, high-wind extreme with a surface maximum of turbulence variables, the turbulence structure first begins to exhibit an elevated maximum, displaced above the surface as the near-surface turbulence and fluxes become weaker. With further increase in stability, the downward turbulence transport occurs in intermittent bursts, as the bulk Ri approaches critical. Even further stabilization produces intermittency that is weaker and in shorter bursts, as the vertical component of the turbulence becomes suppressed with respect to the horizontal components. As the Ri_B increases past critical, the "collapse" of the SBL and vertical component of the turbulence becomes literal, as the depth of the weak, intermittently turbulent boundary layer only reaches on the order of 10 m for the very stable case. Van de Wiel (2003) points out that this one-dimensional analysis is only valid for constant and relatively strong surface cooling R_{net}, and that the regimes are also a function of R_{net}, or the surface cooling potential, which is strongly controlled by cloud cover in general.

A further aspect of these studies is that stability regimes could be discerned using the speed of the LLJ U_x. The category boundaries found here probably are related to strong surface thermal forcing and resultant strong stability near the surface routinely found in this relatively arid region at night. In other studies currently under investigation, there are some indications that in moister locations, the category boundaries shift to smaller values of U_x, emphasizing a need to consider the stability $\partial\theta/\partial z$, which is of course included in Ri_B or Ri_J categorization.

U_x is an external dynamic variable, with respect to the SBL. Defining a stability variable, such as Ri_B also requires a thermodynamic stratification expression. The appropriate external thermodynamic variable, to characterize the stability, in some studies has included the net radiation at the surface (Mahrt *et al*. 2001, van de Wiel 2002b, 2003), but van de Wiel (2002a) has pointed out that the heat flux into the ground or canopy layer is also an important external process in the surface energy budget, so it seems important to include both 'cooling potential' terms in defining an external stability variable.

Of course the subject of discussion is the stable boundary layer of the atmosphere, and the straightforward idealized picture of even the extreme regimes is observed to be interrupted by various kinds of traveling disturbance, which Mahrt refers to as mesoscale disturbances (e.g., Mahrt and Vickers 2006). These are not mixed out as they would be during daytime, because of the suppression of mixing by the stable stratification. Even on strong-wind nights, variations in the speed of the LLJ are noted, and at times a layer of cold air has been observed to be advected in at low levels, perhaps from nearby lower-level terrain, shutting off the surface turbulence, and complicating the simple idealized picture of SBL evolution we are trying to develop. As the Ri_B nears "critical", intermittent processes may be either imported mesoscale disturbances or may be reflecting internal dynamics of the SBL. Such nonstationary processes probably need to be studied on a case-by-case basis to answer important questions, such as: What is the role of these disturbances in the evolution of mean vertical profiles – do they pass through leaving the basic SBL structure essentially unchanged, or do they perform significant vertical mixing?

Acknowledgments. Support for the analysis in this study, which has taken place over several years' time, came from a number of sources, including the U.S. Army Research Office (ARO, Dr. Walter Bach) of the Army Research Laboratory under Proposal No. 43711-EV, and the National Renewable Energy Research Laboratory (NREL, Dr. Neil D. Kelley) of the U.S. Department of Energy (DOE) under Interagency Agreement DOE-AI36-03GO13094. Further analysis and manuscript preparation were supported by the NOAA Air Quality and Health of the Atmosphere program. Field data acquisition for the Lamar project was funded by DOE/NREL. Field data acquisition for the CASES-99 project was supported by ARO under Proposal 40065-EV, the Cooperative Institute for Research in the Atmosphere (Center for Geosciences/Atmospheric Research), and the National Science Foundation under Grant #ATM-9908453. The author is indebted to his colleagues from the NOAA/ESRL lidar optical remote sensing group for contributions to HRDL preparation and setup and data acquisition during CASES and Lamar, including Alan Brewer, Volker Wulfmeyer, Scott Sandberg, Janet Machol, Brandi McCarty, Joanne George, Raul Alvarez, Andreas Muschinski, Jennifer Keane, Ann Weickmann, Ron Richter, R.M. Hardesty, J. Otten, W. Eberhard, M. Pichugin, and Lisa Darby. We also thank Ms. Darby for helpful manuscript reviews and figure preparation. This study has benefited from discussions with Drs. Larry Mahrt, Bas van de Wiel, and Sara Tucker, and special appreciation to Drs. Y.L. Pichugina and R.K. Newsom for acquisition and analysis of the field data.

References

Andreas, E.L, K.J. Claffey, and A.P. Makshtas (2000), Low-level atmospheric jets and inversions over the western Weddell Sea, *Bound.-Layer Meteor*. **97**, 459-486.

Balsley, B.B., R.G. Frehlich, M.L. Jensen, and Y. Meillier (2006), High-resolution in-situ profiling through the stable boundary layer: Examination of the SBL top in terms of

minimum shear, maximum stratification, and turbulence decrease, *J. Atmos. Sci*. **63**, 1291-1307.

Banta, R.M., C.J. Senff, A.B. White, M. Trainer, R.T. McNider, R.J. Valente, S.D. Mayor, R.J. Alvarez, R.M. Hardesty, D.D. Parish, and F.C. Fehsenfeld (1998), Daytime buildup and nighttime transport of urban ozone in the boundary layer during a stagnation episode, *J. Geophys. Res*. **103**, 22,519-22,544.

Banta, R.M., R.K. Newsom, J.K. Lundquist, Y.L. Pichugina, R.L. Coulter, and L. Mahrt (2002), Nocturnal low-level jet characteristics over Kansas during CASES-99, *Bound.-Layer Meteor*. **105**, 221-252.

Banta, R.M., Y.L. Pichugina, and R.K. Newsom (2003), Relationship between low-level jet properties and turbulence kinetic energy in the nocturnal stable boundary layer, *J. Atmos. Sci.* **60**, 2549-2555.

Banta, R.M., N.D. Kelley, and Y.L. Pichugina (2004), Low-level jet properties and turbulence below the jet during the Lamar Low-Level-Jet Project, *16th Symposium on Boundary Layers and Turbulence, Portland ME*, Paper 4.10, 4 pp. (preprints)

Banta, R.M., Y.L. Pichugina, and W.A. Brewer (2006), Turbulent velocity-variance profiles in the stable boundary layer generated by a nocturnal low-level jet, *J. Atmos. Sci*. **63**, 2700-2719.

Banta, R.M., L. Mahrt, D. Vickers, J. Sun, B. Balsley, Y. Pichugina, and E. Williams (2007), The very stable boundary layer on nights with weak low-level jets, *J. Atmos. Sci*. **64** (in press).

Beyrich, F. (1997), Mixing height estimation from sodar data – A critical discussion, *Atmos. Environ*. **31**, 3941-3953.

Blackadar, A.K. (1957), Boundary layer wind maxima and their significance for the growth of nocturnal inversions, *Bull. Amer. Meteor. Soc*. **38**, 283-290.

Blumen, W., R.M. Banta, S.P. Burns, D.C. Fritts, R. Newsom, G.S. Poulos, and J. Sun (2001), Turbulence statistics of a Kelvin-Helmholtz billow event observed in the nighttime boundary layer during the CASES-99 field program, *Dynamics of Atmos. and Oceans* **34**, 189-204.

Bonner, W.D. (1968), Climatology of the low level jet, *Mon. Wea. Rev.* **96**, 833-850.

Brost, R.A., and J.C. Wyngaard (1978), A model study of the stably stratified planetary boundary layer, *J. Atmos. Sci*. **35**, 1427-1440.

Brown, S.S., W.P. Dubé, H.D. Osthoff, D.E. Wolfe, W.M. Angevine, and A.R. Ravishankara (2007), High-resolution vertical distributions of NO_3 and N_2O_5 through the nocturnal boundary layer, *Atmos. Chem. Phys*. **7**, 139-149.

Browning, K.A., and R. Wexler (1968), The determination of kinematic properties of a wind field using Doppler radar, *J. Appl. Meteor.* **7**, 105-113.

Caughey, S.J., J.C. Wyngaard, and J.C. Kaimal (1979), Turbulence in the evolving stable boundary layer, *J. Atmos. Sci*. **36**, 1041-1052.

Drobinski, P., P. Carlotti, R.K. Newsom, R.M. Banta, R.C. Foster, and J.-L. Redelsperger (2004), The structure of the near-neutral atmospheric surface layer, *J. Atmos. Sci*. **61**, 699-714.

Drobinski, P., P. Carlotti, J.-L. Redelsperger, R.M. Banta, V. Masson, and R.K. Newsom (2007), Numerical and experimental investigation of the neutral atmospheric surface layer, *J. Atmos. Sci*. **64**, 137-156.

Emeis, S., M. Harris, and R.M. Banta (2007), Boundary-layer anemometry by optical remote sensing for wind energy applications, *Meteor. Zeitschr*. **16**, 337-347.

Fritts, D.C., C. Nappo, C.M. Riggin, B.B. Balsley, W.E. Eichingre, and R.K. Newsom (2003), Analysis of ducted motions in the stable nocturnal boundary layer during CASES-99, *J. Atmos. Sci*. **60**, 2450-2472.

Grachev, A., C.W. Fairall, P.O.G. Persson, E.L. Andreas, and P.S. Guest (2005), Stable boundary layer scaling regimes: The SHEBA data, *Bound.-Layer Meteor*. **116**, 201-235.

Grund, C.J., R.M. Banta, J.L. George, J.N. Howell, M.J. Post, R.A. Richter, and A.M. Weickmann (2001), High-resolution Doppler lidar for boundary-layer and cloud research, *J. Atmos. Ocean. Technol.* **18**, 376-393.

Ha, K.-J., and L. Mahrt (2001), Simple inclusion of z-less turbulence within and above the modelled nocturnal boundary layer, *Mon. Wea. Rev*. **129**, 2136-2143.

Hanna, S.R. (1969), The thickness of the planetary boundary layer, *Atmos. Environ*. **3**, 519-536.

Hoecker, W.H. (1963), Three southerly low-level jet systems delineated by the Weather Bureau special pibal network of 1961, *Mon. Wea. Rev*. **91**, 573-582.

Holtslag, A.A.M., and F.T.M. Nieuwstadt (1986), Scaling the atmospheric boundary layer. *Bound.-Layer Meteor.* **36**, 201-209.

Kelley, N.D., M. Shirazi, D. Jager, S. Wilde, J. Adams, M. Buhl, P. Sullivan, and E. Patton (2004), Lamar Low-Level Jet Project Interim Report. NREL/TP-500-34593. Golden, CO, National Renewable Energy Laboratory.

Lundquist, J.K. (2003), Intermittent and elliptical inertial oscillations in the atmospheric boundary layer, *J. Atmos. Sci*. **60**, 2661-2673.

Mahrt, L. (1981), Modelling the depth of the stable boundary layer, *Bound.-Layer Meteor*. **21**, 3-19.

Mahrt, L. (1998), Stratified atmospheric boundary layers and breakdown of models, *J. Theor. Comp. Fluid Dyn*. **11**, 263-280.

Mahrt, L. (1999), Stratified atmospheric boundary layers, *Bound.-Layer Meteor*. **90**, 375-396.

Mahrt, L., and D. Vickers (2002), Contrasting vertical structures of nocturnal boundary layers, *Bound.-Layer Meteor*. **105**, 351-363.

Mahrt, L., and D. Vickers (2006), Extremely weak mixing in stable conditions, *Bound.-Layer Meteor*. **119**, 19-39.

Mahrt, L., R.C. Heald, D.H. Lenschow, B.B. Stankov, and I. Troen (1979), An observational study of the structure of the nocturnal boundary layer, *Bound.-Layer Meteor*. **17**, 247-264.

Mahrt, L., J. Sun, W. Blumen, T. Delaney, and S. Oncley (1998), Nocturnal boundary layer regimes, *Bound.-Layer Meteor.* **88**, 255-278.

Mahrt, L., D. Vickers, R. Nakamura, M.R. Soler, J. Sun, S. Burns, and D.H. Lenschow (2001), Shallow drainage flows, *Bound.-Layer Meteor.* **101**, 243-260.

McNider, R.T., M.D. Moran, and R.A. Pielke (1988), Influence of diurnal and inertial boundary-layer oscillations on long-range dispersion, *Atmos. Environ*. **11**, 2445-2462.

Mitchell, M.J., R.W. Arritt, and K. Labas (1995), A climatology of the warm season Great Plains low-level jet using wind profiler observations, *Wea. Forecasting* **10**, 576-591.

Newsom, R.K., and R.M. Banta (2003), Shear-flow instability in the stable nocturnal boundary layer as observed by Doppler lidar during CASES-99, *J. Atmos. Sci*. **30**, 16-33.

Newsom, R.K., and R.M. Banta (2004a), Assimilating coherent Doppler lidar measurements into a model of the atmospheric boundary layer. I: Algorithm development and sensitivity to measurement error, *J. Atmos. Ocean. Technol*. **21**, 1328-1345.

Newsom, R.K., and R.M. Banta (2004b), Assimilating coherent Doppler lidar measurements into a model of the atmospheric boundary layer. II: Sensitivity analyses, *J. Atmos. Ocean. Technol*. **21**, 1809-1824.

Nieuwstadt, F.T.M. (1984), The turbulent structure of the stable, nocturnal boundary layer, *J. Atmos. Sci*. **41**, 2202-2216.

Obukhov, A.M. (1971), Turbulence in an atmosphere with a non-uniform temperature, *Bound.-Layer Meteor*. **2**, 7-29.

Ohya, Y. (2001), Wind-tunnel study of atmospheric stable boundary layers over a rough surface, *Bound.-Layer Meteor*. **98**, 57-82.

Ohya, Y., D.E. Neff, and R.N. Meroney (1997), Turbulence structure in a stratified boundary layer under stable conditions, *Bound.-Layer Meteor.* **83**, 139-161.

Pichugina, Y.L., R.M. Banta, N.D. Kelley, S.P. Sandberg, J.L. Machol, and W.A. Brewer (2004), Nocturnal low-level jet characteristics over southeastern Colorado, *16th Symposium on Boundary Layers and Turbulence, Portland ME*, Paper 4.11, 6 pp. (preprints).

Pichugina, Y.L., R.M. Banta, W.A. Brewer, N.D. Kelley, R.K. Newsom, and S.C. Tucker (2008), Evaluation of Doppler-lidar-based horizontal-velocity and turbulence profiles to averaging procedures, *J. Atmos. Ocean. Technol*. **24** (submitted).

Poulos, G., W. Blumen, D.C. Fritts, J.K. Lundquist, J. Sun, S.P. Burns, C. Nappo, R, Banta, R. Newsom, J. Cuxart, E. Terradellas, B. Balsley, and M. Jensen (2002), CASES-99: A comprehensive investigation of the stable nocturnal boundary layer, *Bull. Amer. Meteor. Soc*. **83**, 555-581.

Seibert, P., F. Beyrich, S.-E. Gryning, S. Joffre, A. Rasmussen, and P. Tercier (2000), Review and intercomparison of operational methods for the determination of the mixing height, *Atmos. Environ*. **34**, 1001-1027.

Smedman, A.-S. (1988), Observations of a multi-level turbulence structure in a very stable atmospheric boundary layer, *Bound.-Layer Meteor.* **44**, 231-253.

Smedman, A.-S., M. Tjernström, and U. Högström (1993), Analysis of the turbulence structure of a marine low-level jet, *Bound.-Layer Meteor*. **66**, 105-126.

Smedman, A.-S., H. Bergström, and B. Grisogano (1997), Evolution of stable internal boundary layers over a cold sea, *J. Geophys. Res*. **102**, 1091-1099.

Song, J., K. Liao, R.L. Coulter, and B.M. Lesht (2005), Climatology of the low-level jet at the Southern Great Plains atmospheric boundary layer experiment site, *J. Appl. Meteor*. **44,** 1593-1606.

Steeneveld, G.J., B.J.H. van de Wiel, and A.A.M. Holtslag (2007), Diagnostic equations for the stable boundary layer height: Evaluation and dimensional analysis, *J. Appl. Meteor. Climate* **46,** 212-225.

Stensrud, D.J. (1996), Importance of the low-level jet to climate, *J. Climate* **9**, 1698-1711.

Sun, J., S.P. Burns, D.H. Lenschow, R.M. Banta, R.K. Newsom, R. Coulter, S. Frasier, T. Ince, C.J. Nappo, J. Cuxart, W. Blumen, X. Lee, and X.-Z. Hu (2002), Intermittent turbulence associated with a density current passage in the stable boundary layer, *Bound.-Layer Meteor*. **105**, 199-219.

Sun, J., D. Lenschow, S. Burns, R. Banta, R. Newsom, R. Coulter, S. Frasier, T. Ince, C. Nappo, B. Balsley, M. Jensen, L. Mahrt, D. Miller, and B. Skelly (2004), Intermittent turbulence in stable boundary layers and the processes that generate it, *Bound.-Layer Meteor.* **110**, 255-279.

van de Wiel, B.J.H., A. Moene, O. Hartogensis, H.A.R. de Bruin, and A.A.M. Holtslag (2002a), Intermittent turbulence in the stable boundary layer over land. Part I: A bulk model, *J. Atmos. Sci*. **59**, 942-958.

van de Wiel, B.J.H., A. Moene, R.J. Ronda, H.A.R. de Bruin, and A.A.M. Holtslag (2002b), Intermittent turbulence in the stable boundary layer over land. Part II: A system dynamics approach, *J. Atmos. Sci*. **59**, 2567-2581.

van de Wiel, B.J.H., A. Moene, O. Hartogensis, H.A.R. de Bruin, and A.A.M. Holtslag (2003), Intermittent turbulence in the stable boundary layer over land. Part III: A classification for observations during CASES-99, *J. Atmos. Sci.* **60**, 2509-2522.

Vickers, D., and L.J. Mahrt (2003), The cospectral gap and turbulent flux calculations, *J. Atmos. Ocean. Technol.* **20**, 660-672.

Vickers, D., and L.J. Mahrt (2004), Evaluating formulations of stable boundary layer height, *J. Appl. Meteor*. 4**3**, 1736-1749.

Vickers, D., and L.J. Mahrt (2006), A solution for flux contamination by mesoscale motions with very weak turbulence, *Bound.-Layer Meteor*. **118**, 431-447.

Vogelezang, D.H.P., and A.A.M. Holtslag (1996), Evaluation and model impacts of alternative boundary-layer height formulations, *Bound.-Layer Meteor*. **81**, 245-269.

Wetzel, P.J. (1982), Toward parameterization of the stable boundary layer, *J. Appl. Meteor*. **21**, 7-13.

Whiteman, C.D., X. Bian, and S. Zhong (1997), Low-level jet climatology from enhanced rawinsonde observations at a site in the Southern Great Plains, *J. Appl. Meteor.* **36**, 1363-1376.

Wulfmeyer, V.O., M. Randall, W.A. Brewer, and R.M. Hardesty (2000), 2 μm Doppler lidar transmitter with high frequency stability and low chirp, *Opt. Lett.* **25**, 1228-1230.

Wyngaard, J.C. (1973), On Surface-Layer Turbulence. Workshop on Micrometeorology, American Meteorological Society, Boston, 101-149.

Wyngaard J.C., and O.R. Coté (1972), Cospectral similarity in the atmospheric surface layer, *Quart. J. Royal Meteor. Soc*. **98**, 590-603.

Zhong, S., and J.D. Fast (2003), An evaluation of the MM5, RAMS, and Meso-Eta models at subkilometer resolution using field campaign data in the Salt Lake Valley, *Mon. Wea. Rev*. **131**, 1301-1322.

Zhong, S., J.D. Fast, and X. Bian (1996), A case study of the Great Plains low-level jet using wind profiler network data and a high-resolution mesoscale model, *Mon. Wea. Rev*. **5**, 785-806.

Zilitinkevich, S. (1972), On the determination of the height on the Ekman boundary layer, *Bound.-Layer Meteor*. **3**, 141-145.

Zilitinkevich, S., and D.V. Mironov (1996), A multi-limit formulation for the equilibrium height of a stably stratified boundary layer, *Bound.-Layer Meteor*. **81**, 141-145.

Received 15 June 2007
Accepted 27 November 2007